Low-energy photoelectron diffraction structure determination of GaSe-bilayer-passivated Si(111)

Shuang Meng, B.R. Schroeder, A. Bostwick, and Marjorie A. Olmstead
Department of Physics, University of Washington, Box 351560, Seattle, Washington 98195

Eli Rotenberg
Advanced Light Source, Lawrence Berkeley National Laboratory, Berkeley, California 94720

F. S. Ohuchi
Department of Material Science and Engineering, University of Washington, Box 352120, Seattle, Washington 98195
(Received 23 January 2001; revised manuscript received 9 July 2001; published 19 November 2001)

The atomic structure of GaSe-bilayer-passivated Si(111) was determined using low-energy photoelectron diffraction (PED). Scanned-energy and scanned-angle PED measurements were combined with multiple-scattering calculations to investigate the specific bonding configuration and to test the applicability of these techniques in an electron energy range where multiple and back scattering are important. Using tunable synchrotron radiation to vary the electron wavelength for emission along the Ga-Si and Ga-Se bonds, we determined the Ga site to be directly atop a surface Si atom with a bond length of 2.35 ± 0.02 Å. We find the Ga-Se bond lies 65° from the surface normal towards $[11\bar{2}]$, with length 2.44 ± 0.01 Å. Diffraction stereograms [variable-angle scattering at constant kinetic energy (KE)] for Ga $3d$ emission (KE = 230 eV) show threefold symmetric, forward-focusing peaks along Ga-Se bonds, indicating a single-domained bilayer. Se $3d$ stereograms (KE = 196 eV) show a sixfold ripple pattern due to scattering from the six in-plane Se next-nearest neighbors. Multiple scattering analysis is required to explain the full diffraction pattern for this two-layer thick film. Polar-angle scans at constant azimuth and kinetic energy were measured using conventional laboratory x-ray sources for Ga $2p$ (KE = 131 eV) and Se $2p$ (KE = 48 eV). The results, subjected to multiple-scattering analysis, are consistent with the structure determined using synchrotron radiation. These results demonstrate low-energy PED as an effective tool in structural determination.

DOI: 10.1103/PhysRevB.64.235314 PACS number(s): 68.35.−p, 79.60.Dp, 79.60.Jv

I. INTRODUCTION

Truncation of covalently-bonded crystals at a surface introduces complexity into their atomic and electronic structures through the creation of dangling bonds. This complexity often manifests itself in geometric reconstructions of the near-surface region and in the appearance of surface electronic states. Removal of surface reconstruction and modification of surface properties can be achieved by introducing extraneous atoms to the surface that passivate surface dangling bonds. The resultant fully coordinated low-energy surface may serve as a stable, unreactive substrate for subsequent growth and processing. In this paper, we detail the structure of such a surface: GaSe-terminated Si(111).

The ideal Si(111) surface would have a single dangling bond per surface atom. This surface reconstructs into the complex 7×7 dimer-adatom-stacking fault reconstruction,[1] which eliminates about 60% of the dangling bonds. Elimination of the reconstruction, plus passivation of the reactive dangling bonds, may be achieved by adding an additional valence electron per surface atom. This was first achieved with hydrogen saturation of the surface dangling bonds [Fig. 1(a)],[2] a technique which has since been improved through wet chemistry.[3,4] Passivation and a 1×1 surface unit cell may also be achieved by replacing the top Si layer with As [Fig. 1(b)].[5,6] The same total of 9 valence electrons in the outermost Si bilayer may also be achieved by replacing it with a Ga-Se bilayer [Fig. 1(c)]. The resultant Si(111):GaSe structure, with Si-Ga bonds and surface Se lone-pair states, is a fully coordinated surface and bears strong resemblance to Si(111):As.[7–10] This surface is highly stable and resistant to contamination.[7,8,11,12] Additional GaSe does not stick to the bilayer at substrate temperatures above 525 °C.[7] In angle resolved photoemission measurements, we have found the electronic structures of the lone pair states on the Si(111):As and Si(111):GaSe surfaces are similar, while the back-bonding states differ significantly. These results will be published elsewhere.[10]

The passivated Si(111):GaSe surface serves as a model system for initiating binary-materials heteroepitaxy. The GaSe bilayer structure is the building block of both bulk gallium-selenium crystal structures—layered GaSe and cubic Ga_2Se_3—although in the cubic form, 1/3 of the Ga sites are empty. Layered GaSe has a lattice spacing 2.4% smaller than that of Si(111), whereas Ga_2Se_3 is lattice matched to Si within 0.3%. Epitaxy of III-VI materials on silicon is attracting increasing interest due to many distinct structural, electronic and optical properties displayed by chalcogenide-

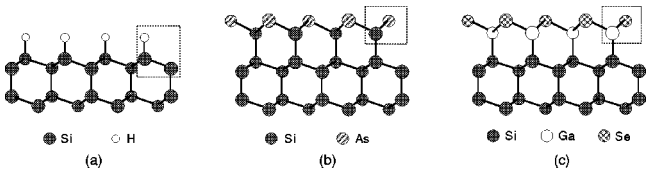

FIG. 1. Atomic structures of the passivated Si(111) surface: (a) Si(111):H, (b) Si(111):As, (c) Si(111):GaSe. Each box in the diagram contains 9 valence electrons.

based semiconductors and their potential use in optoelectronic devices.[13] Several groups have reported growth of layered GaSe on Si(111).[8,9,14–19]

A full understanding of the properties and passivation behavior of the Si(111):GaSe surface requires detailed knowledge of its structure. Previous experiments using x-ray standing wave fluorescence (Ref. 9) and high-kinetic-energy photoelectron diffraction (Ref. 7) are consistent with the structure shown in Fig. 1(c), reporting a Ga-Si distance of 2.37 ± 0.03 Å (Ref. 9) and a Ga-Se bond angle of 64° (7). The x-ray measurements, however, were on air-exposed samples and appeared to support multiple orientations of the Ga-Se bond.[8,9]

In this paper, we present a low-energy photoelectron spectroscopy and diffraction study of GaSe-bilayer passivated Si(111). High resolution core-level spectroscopy shows the Ga and Se atoms to occupy single environments, while the interface Si is found to be in a very bulklike environment. Using scanned-energy photoelectron diffraction measurements, combined with multiple-scattering theoretical analysis, we determine that Ga resides 2.35 ± 0.02 Å above surface Si atoms, while the Ga-Se bond parameters are between those of the two bulk crystal structures. This is consistent with both previous experimental results and with an unpublished density-functional structural calculation.[20] We also utilized this ideal heteroepitaxial system to test photoelectron diffraction modeling for covalently-bonded surfaces with multiple atomic species. At kinetic energies near 200 eV, Ga PED is dominated by forward focusing along the three Ga-Se bonds, while Se PED displays diffraction rings from in-plane scattering.

II. EXPERIMENTAL AND THEORETICAL CONFIGURATION

Photoelectron diffraction measurements were conducted using both synchrotron [advanced light source (ALS) beamline 7.01] and laboratory (Seattle) sources. *N*-type Si(111) substrates ($\rho \sim 1\ \Omega$ cm) were outgassed at 500 °C and then flashed to 875 °C until a sharp 7×7 low-energy electron diffraction (LEED) pattern was observed. GaSe was subsequently deposited at substrate temperature $T_s = 550$ °C with a GaSe Knudsen cell. The deposition time is not critical, since only a single GaSe bilayer sticks at this temperature. The detailed sample preparation procedure has been reported elsewhere.[7] After deposition, samples were transported under UHV conditions from the preparation chamber (base pressure 7×10^{-11} Torr in Seattle and 2×10^{-10} at the ALS) to the analysis chamber (base pressure 1×10^{-10} Torr). Photoelectron diffraction measurements were performed on a double rotating stage in the analysis chamber. At the synchrotron, the angle between the incident photons and detected electrons was fixed at 60° in the horizontal plane and the sample was rotated around the horizontal axis (θ) and the sample normal (ϕ). The photons were polarized in the horizontal plane. In Seattle, the angle between the incident Mg K_α or Al K_α photons and the detected electrons was fixed at 55° in the horizontal plane. The sample rotated around the vertical axis (θ) and the sample normal (ϕ). Data are presented in crystal coordinates (ϕ measured counterclockwise from $[11\bar{2}]$, θ measured from sample normal).

Photoelectron diffraction (PED) probes local atomic structure through variation of photoemitted electron intensities with wave vector $\vec{k}$. This variation arises from interference between the portion of the electron wave traveling directly to the detector and the portion scattered by nearby atoms. At high kinetic energies (KE > 500 eV), forward scattering dominates, and the primary intensity variation is with emission direction. In this paper, we exploit the enhanced back-scattering amplitude at lower kinetic energy to obtain information about the location of the GaSe bilayer relative to the Si substrate. Experiments varied the electron wave vector's magnitude and angle through the photon energy and sample orientation, respectively.

Below about 300 eV kinetic energy, the large scattering cross section, combined with comparable scattering intensity in forward and backward directions, means that multiple-scattering analysis is crucial to interpreting photoelectron diffraction measurements. We performed low-energy PED modeling using the code MSCD,[21] which applies the Rehr-Albers separable representation of spherical-wave propagators[22] to a multiple-scattering cluster calculation. Calculations were carried out up to fourth order in Rehr-Albers expansion and to eighth order in multiple scattering. Phase shifts (for electron waves scattering off atoms) were calculated using the *ab initio* EXAFS code FEFF.[23] Calculations were performed for a paraboloid cluster of 121 atoms, representing a strained GaSe bilayer terminated Si(111) surface with no reconstruction. The code is based on a spherical local potential, but includes charge redistribution in the partially ionic bonds. The effect of the nonspherical covalent bonds in photoelectron diffraction is expected to be quite small for the kinetic energies used here,[24] which are at least 40 eV above the vacuum level.

III. EXPERIMENTAL RESULTS AND DISCUSSIONS

A. Substrate modification

The effectiveness of GaSe bilayer passivation and its influence on the Si(111) substrate can be examined by low-energy electron diffraction and surface sensitive photoemission spectroscopy. The surface LEED pattern changes from the characteristic Si(111) 7×7 pattern to a post-growth 1×1 pattern with strong and sharp diffraction spots. This indicates a well-ordered structure that completely removes the 7×7 reconstruction.

Surface sensitive Si $2p$ core-level photoemission, shown in Fig. 2 reveals all near-surface silicon atoms to be in a bulklike environment. The figure shows Si $2p$ spectra at two photon energies, with electron escape depths of approximately 3.5 Å ($h\nu = 150$ eV) and 5.5 Å ($h\nu = 250$ eV), and two angles. The two spectra at $h\nu = 250$ eV are normalized to the total flux on the sample, all of which fell within the measurement area of the electron detector as the spot size increased with angle. The solid line is a fit to the $h\nu = 150$ eV data with a single-component, spin-orbit Voigt function (spin-orbit splitting $= 0.607$ eV, spin-orbit ratio

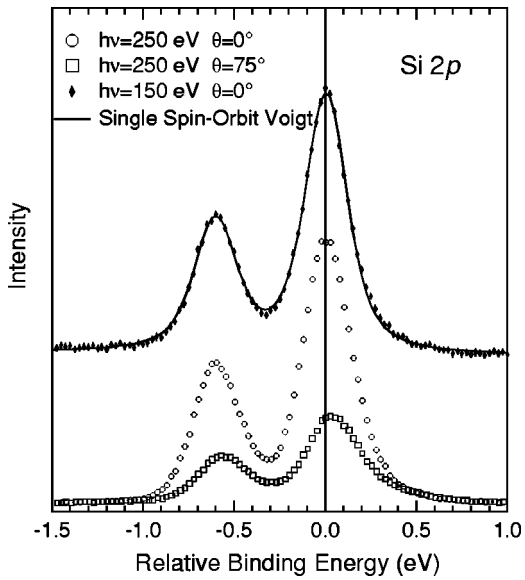

FIG. 2. Surface sensitive Si $2p$ photoemission spectra. Solid line indicates the fitted spin-orbit Voigt function.

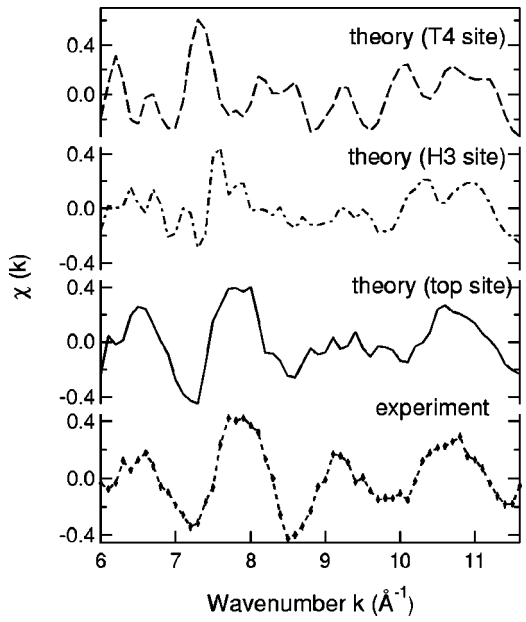

FIG. 3. Ga $3d$ intensity modulation versus photoelectron wave number in scanned-energy PED along surface normal ($\theta=0°, \phi=0°$). The bottom curve shows experimental data; the upper three curves are theoretical calculations for Ga residing above the second layer Si (T_4 site), above the fourth layer Si (H_3 site), or above the surface Si (top site).

$=0.506$, Lorenztian FWHM $=0.13$ eV, Gaussian FWHM $=0.20$ eV). At high polar angles, the peak shows a slight broadening (to Gaussian FWHM 0.27 eV) and a shift of about 30 meV to lower binding energy. Any component due to the interface Si would be largest in this spectrum, as the bulk emission is attenuated by inelastic scattering. The shift and broadening could indicate a small surface shift to lower binding energy. The energy splitting between the bulk and surface components can be determined to be no more than 200 meV, less than the surface shift ($\sim$300 meV) observed on the Si(111):Ga$\sqrt{3}\times\sqrt{3}$ surface.[25] By contrast, the Si(111):As system exhibits a 0.75 eV shifted component in the Si $2p$ spectra, due to charge transfer in the Si-As bonds.

Another possible contribution to the observed shift to lower binding energy at high angles is the surface photovoltage effect. On these passivated samples with only a few defect states in the energy gap, increased photon flux, and the resultant increase in electron-hole pair density near the surface, causes the bands to flatten. The light intensity is roughly four times higher at normal emission than at 75°. For these *n*-type samples, flatter bands means the core levels are then further from the Fermi energy (higher binding energy) for a smaller photon spot ($\theta=0°$). Ga $3d$ and Se $3d$ core-level spectra were also measured at the same photon energies. Both spectra (not shown) show a single component within our resolution. In the range from 60°–85° emission (obtained by rotating the sample in the photon beam), the Si, Ga, and Se peaks all show a similar 20–30 meV shift to lower binding energy with increasing angle. This supports a photovoltaic contribution to the observed shift with angle.

B. Scanned energy photoelectron diffraction

The observed threefold symmetric, 1×1 LEED pattern requires the Ga overlayer to reside in one of the three high-symmetry Si(111) bonding sites: top (above first layer Si), H_3 (above fourth layer Si), or T_4 (above second layer Si) sites. The local structural environment exerts a strong influence on the Ga core-level intensity as a result of interference between direct and backscattered electron waves. Figure 3 shows the measured normal-emission Ga $3d$ photoelectron intensity modulation versus photoelectron wave number. The measurements were carried out at a succession of photon energies between 156 and 532 eV, with the energy increment chosen to correspond to a photoelectron wave vector increment of 0.1 Å^{-1}. Ga $3d$ core-level spectra were recorded at each energy and subsequently curve-fitted to extract intensities $I(k)$. The intensity modulation χ shown in Fig. 3 was then obtained from the following expression:

$$\chi(k)=[I(k)-I_0(k)]/I_0(k),$$

where $I_0(k)$ is a smooth background function obtained from a cubic-spline fit to the intensity function $I(k)$.

The upper three curves in Fig. 3 correspond to theoretical multiple-scattering calculations for the bilayer structure with Ga in the T_4, H_3 and top site configurations, respectively. The vertical Si-Ga plane spacings for these calculations were taken from x-ray standing wave results for the Ga-Se bilayer (top site, 2.37 Å) (Ref. 9) and for Si(111):Ga$\sqrt{3}\times\sqrt{3}$—$R30°$ (T_4 and H_3, 1.82 Å).[26] The Ga-Se bond was assumed in all cases to be that determined for the GaSe bilayer using high-energy photoelectron diffraction.[7]

The theoretical modeling predicts significant differences in the measured diffraction patterns for the three bonding configurations. The best agreement, as is apparent in Fig. 3, is obtained for the configuration in which Ga sits directly atop surface Si. Adjusting the Ga-Si interlayer separation in

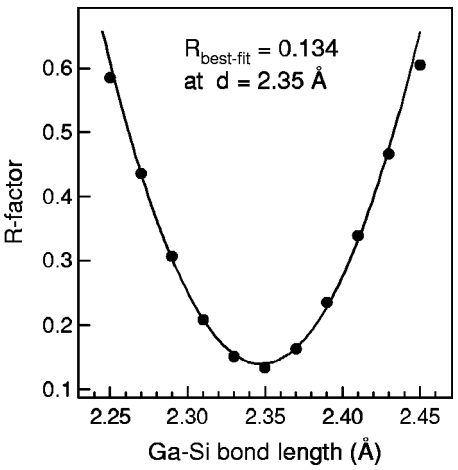

FIG. 4. Reliability factors of fit between the scanned-energy PED experiment and the theory for top site configuration as a function of Ga-Si bond length. The solid line is a fitted parabola through the data points, with a minimum at 2.35 Å.

the cases of T_4 and H_3 configurations does not lead to significant improvement in the fit.

In normal emission, the observed intensity oscillations with wave number arise primarily from interference between direct (unscattered) Ga emission and emission backscattered from the underlying Si. The dominant feature of the data is an oscillation with period ~ 1.3 Å^{-1}, corresponding to a real-space path difference of ~ 4.8 Å. This distance is most consistent with Ga in the top site, being approximately twice the expected bond length. This result may be optimized by comparing theory and experiment as a function of Ga-Si bond length. Figure 4 shows the reliability factors of fit, or R factors, for the top site configuration, with R given by[21]

$$R = \frac{\sum_i (\chi_{ci} - \chi_{ei})^2}{\sum_i (\chi_{ci}^2 + \chi_{ei}^2)},$$

where χ_{ci} and χ_{ei} are calculated and experimental χ curves, respectively. The inner potential was also fitted and then set to the best-fit value of 12 eV. This compares to a value of about 14 ± 2 eV obtained using normal-emission variable photon energy valence band spectroscopy (locating the top of the Si valence band at Γ in the third Brillouin zone).[10] In the case of PED, the inner potential is given by the value of the potential between the atoms (referred to as the ''muffin-tin zero''); for photoemission, it is the potential step required for the perpendicular momentum to match known symmetry points in the Si bulk band structure. The R factors show a symmetric parabola with minimum at 2.35 ± 0.02 Å. This result is within the error bars of the Ga-Si bond length of 2.37 Å deduced by XSWF,[9] and of 2.36 Å obtained in a DFT calculation of the Si(111):GaSe structure.[20] Figure 5 shows the structure deduced from both this measurement and that described below using Se $3d$ emission.

Figure 6 shows a measurement of the Se $3d$ χ function versus electron wave vector along the Ga-Se bond direction

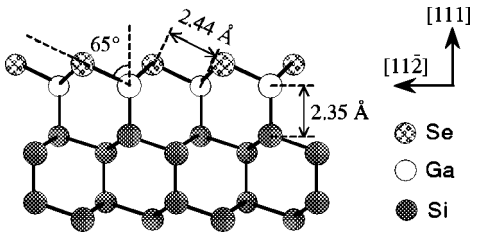

FIG. 5. Schematic of the GaSe bilayer structure on Si(111) substrate deduced from the Ga $3d$ and Se $3d$ scanned-energy PED experiments.

($\sim 64°$ from the surface normal). The strong intensity modulation evident in the data is largely due to interference between direct Se emission and emission backscattered from Ga along the Se-Ga bond. The inset in Fig. 6 shows the R factors of fit between experiment and theory as a function of the assumed Ga-Se bond length. The theoretical calculations were carried out using the same parameters as in the Ga case with the exception of the surface Debye temperature. The Ga $3d$ data could be well fitted with $T_{\mathrm{Debye}} = 625$ K, the value for bulk Si, where as for the Se emission the best fit is for $T_{\mathrm{Debye}} = 425$ K.

The ratio of the measurement temperature (300 K) to the Debye temperature characterizes the distribution of atomic positions around their average values. Since photoemission occurs on a time scale quite short relative to atomic vibrations, both static disorder and increased vibrational amplitude may be simulated through a decreased Debye temperature. It is likely both play a role here. The Se atom environment for this surface is very similar to that of As on As-terminated Si(111). Medium energy ion scattering

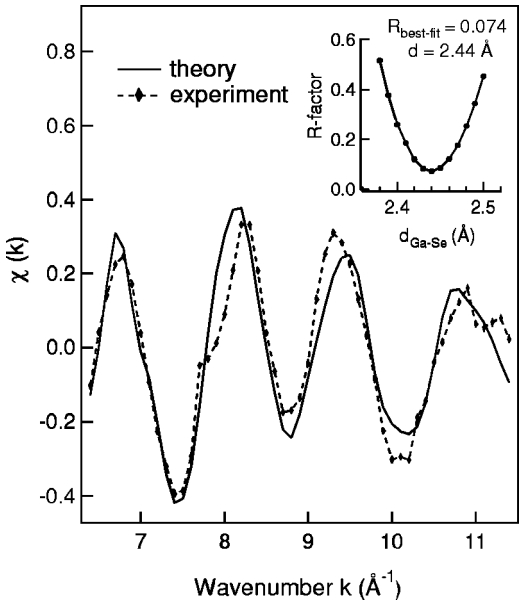

FIG. 6. Se $3d$ intensity modulation versus photoelectron wave number in scanned-energy PED along the Ga-Se bond direction ($\theta = 64°, \phi = 0°$). The inset shows R factors of fit between experiment and theory as a function of Ga-Se bond length. The best-fit value is 2.44 Å. Solid curve indicates the corresponding theoretical calculation using this bond length.

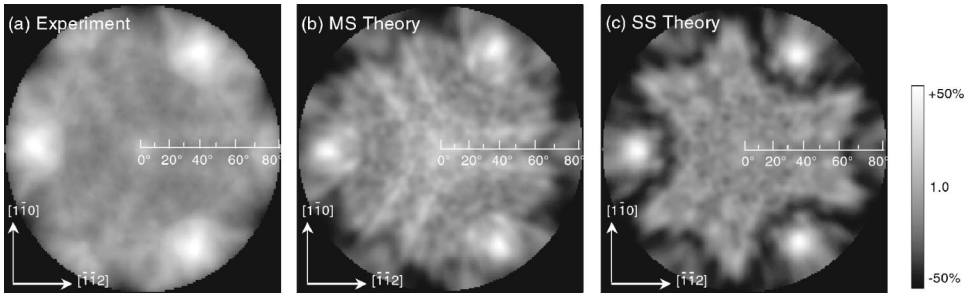

FIG. 7. Stereographic projections of Ga $3d$ photoemission intensity (stereograms) from Si(111):GaSe at $h\nu=246$ eV (KE$=226$ eV). (a) Experimental measured PED stereogram. Data were collected in a 140° azimuthal section and subsequently symmetrized. (b) Multiple-scattering calculation of the PED stereogram (MS order$=4$, RA order$=2$). (c) Single-scattering calculation of the PED stereogram (MS order$=1$, RA order$=0$). Polar angles are labeled on the superimposed radial scales. The gray scale bar on the right indicates intensity variations.

(MEIS) data for Si(111):As show a similar enhanced displacement of As atoms from their equilibrium positions.[27,28] The MEIS data have been interpreted both in terms of an enhanced vibrational amplitude (80% larger than expected for bulk vibrations)[27] and in terms of significant static disorder (20% of the As atoms randomly located).[28] Temperature-dependent x-ray standing wave results for Ga and As monolayers on Si(111)[29] show similarly enhanced vibrational amplitudes at room temperature that increase further with temperature, indicating a major vibrational component to the displacements.

Reducing the effective Debye temperature does not affect the periodicity of the photoelectron diffraction modulation, and hence not the fitted bond length. However, it does improve the overall amplitude agreement between theory and experiment. The effect of disorder is strongest at high values of k, and the decrease in quality of fit at higher k values is likely due to the inadequacies of a simple harmonic model in accounting for the local atomic displacements. Another source of discrepancies between experiment and theory is the difficulty in accurately extracting the χ function at higher photon energies (high k), where the cross section for Se $3d$ emission is about one twentieth that at the peak.

The best-fit to the data in Fig. 6 was obtained at a Ga-Se bond length of 2.44 ± 0.01 Å, corresponding to bond angle of 65.3° from the surface normal (see Fig. 5). This value is $\sim1°$ larger than the value previously determined using scanned-angle high energy XPD,[7] but is within the error bars of the previous measurement. It also compares well with the DFT result of 2.47 Å(63.9°),[20] which implies that the anharmonic effects which typically lengthen effective bond lengths relative to $T=0$ are small. The solid line in Fig. 6 reflects the theoretical prediction using the best-fitted GaSe bond length.

C. Scanned angle photoelectron diffraction

1. Medium kinetic energy 3d emission

In the previous section, we described variations in photoemission intensity with electron wave vector magnitude at constant angle. Here, we obtain additional information about the local structural environment of the Ga and Se atoms in the bilayer by varying the direction of the photoelectron wave vector at constant magnitude. Figures 7(a) and 8(a) show measured stereographic projections of the Ga and Se $3d$ photoemission intensity at photon energy $h\nu=246$ eV (Ga KE$=230$ eV, $k=7.77$ Å^{-1}; Se KE$=196$ eV, $k=7.17$ Å^{-1}). For each projection, 1404 data points were sampled in a 140° azimuthal section (polar angle θ between normal emission and 80°) and then symmetrized to produce the 360 degree stereographic projection. The sampled points were evenly distributed in solid angle. At each data point,

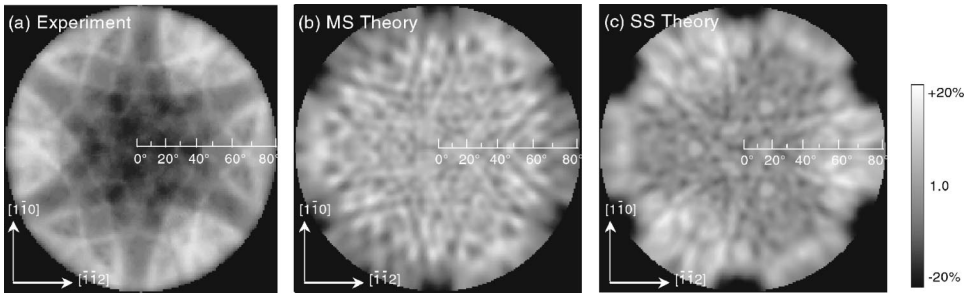

FIG. 8. Stereographic projections of Se $3d$ photoemission intensity (stereograms) from Si(111):GaSe at $h\nu=246$ eV (KE$=192$ eV). (a) Experimental measured PED stereogram. Data were collected in a 140° azimuthal section and subsequently symmetrized. (b) Multiple-scattering calculation of the PED stereogram (MS order$=4$, RA order$=2$). (c) Single-scattering calculation of the PED stereogram (MS order$=1$, RA order$=0$). Polar angles are labeled on the superimposed radial scales. The gray scale bar on the right indicates intensity variations.

intensities were recorded at the binding energy corresponding to the photoemission peak position, specifically, 20.0 eV below the Fermi level for Ga 3*d* and 54.5 eV for Se 3*d*, and at a reference point on the low binding energy side of each photoemission peak. The signal in Figs. 7(a) and 8(a) is the difference between the peak and background intensity.

Figures 7(b) and 8(b) show the calculated projections for Ga and Se 3*d* photoemission intensities based on multiple-scattering theory. The input clusters use the structural parameters deduced in the previous section. The calculations were carried out in fourth-order multiple-scattering (MS) and second-order Rehr-Albers (RA) approximation.[21,22] We found the calculations reach excellent convergence at these orders. Angular stepsizes were set at 1° in polar and 2° in azimuthal directions. Corresponding single-scattering calculations are also included and shown in Figs. 7(c) and 8(c). These calculations were performed only keeping the first-order of MS and zeroth-order of RA, which is equivalent to a single-scattering model in point-scattering approximation.[22]

The Ga 3*d* emission exhibits strong diffraction peaks along the three Ga-Se bonds, indicating forward focusing still dominates at this energy. Backscattering can also be observed in Fig. 7 along the surface normal. At this energy, the Ga-Si backscattering χ is near a maximum (see Fig. 3). The clear threefold symmetry, with no forward scattering along the $[\bar{1}\bar{1}2]$ axes, confirms the existence of a single domain. The calculated Ga stereogram reproduces the main experimental features, confirming the deduced structure. A threefold double line feature can be seen in both measured stereogram image and the multiple-scattering calculation starting from the center and running radially toward the outer edge. It is absent from the single-scattering calculation [Fig. 7(c)] and, therefore, indicates a multiple-scattering effect.

The Se 3*d* emission displays no strong diffraction features, consistent with Se forming the top layer of the bilayer structure (see Fig. 5). A sixfold ripple pattern can be seen in the experimental stereogram image. This ripple pattern arises from scattering off the six in-plane Se next-nearest neighbors. It is apparent from Fig. 8 that the single-scattering calculation is not adequate in reproducing the experimental image. Multiple-scattering calculations, however, do show a similar sixfold diffraction pattern, although there are more fine features, especially near the central region. The absence of these fine features in the experimental stereogram may be due to either static disorder or dynamic Debye-Waller effects. Such effects impact the Se stereogram images more than the Ga ones, due to the absence of strong diffraction features in Se stereograms. A weak threefold enhancement of intensity near 65° is present in both experimental and calculated Se stereograms. This enhancement is due to backscattering from Ga nearest neighbors (see Fig. 6).

2. Low kinetic energy 2p emission

At lower kinetic energies ($\leqslant$150 eV), forward focusing no longer dominates the diffraction pattern and backscattering is significantly enhanced. Structural information may be obtained through comparison of measured angular intensity variations with multiple scattering calculations. We have performed such low-energy scanned-angle PED measurements of Ga and Se 2*p* core-level photoemission using a double anode (Mg/Al) x-ray source. The results confirm both the structural model in Fig. 5 and the applicability of multiple-scattering theory to a two-layer film. They also demonstrate the possibility of using a laboratory-based source to perform backscattering-based structural measurements.

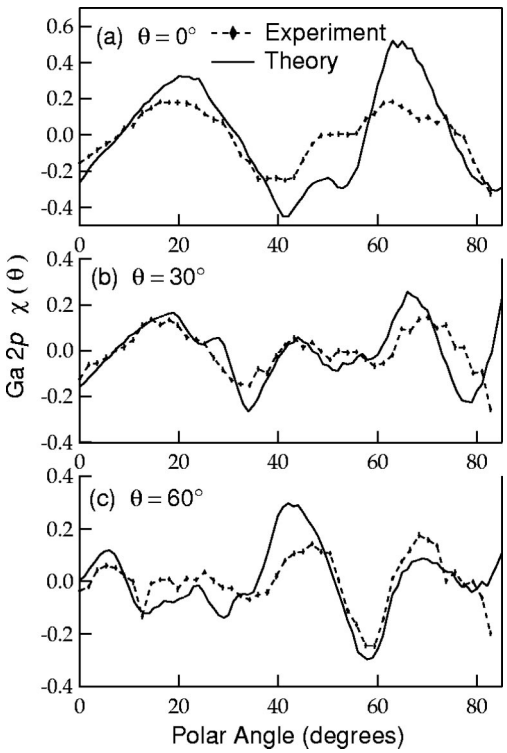

FIG. 9. Ga 2*p* (KE=131 eV) photoelectron intensity modulations vs polar angle along three high symmetry azimuths: 0°, 30°, and 60°, corresponding to $[11\bar{2}]$, $[10\bar{1}]$, and $[2\bar{1}\bar{1}]$ azimuths, respectively.

Figure 9 shows the polar-angle intensity variation of Ga 2*p* 3/2 emission along three high symmetry azimuths. The kinetic energy of the ejected photoelectrons is around 131 eV for these Mg K_α x rays ($h\nu$=1253.6 eV). The measured low-energy XPD patterns for Ga show rather complex features, in contrast to the high energy XPD pattern shown in Ref. 7. Low-energy XPD patterns generally contain more information than high energy ones, owing to enhanced multiple-scattering and backscattering effects. Low energy XPD has been widely used to extract adsorbate positions on substrates.[26]

The solid lines in Fig. 9 are multiple-scattering calculations based on an unpolarized light source, a 3° detector half-angle, and the structure model in Fig. 5. Theoretical χ functions were extracted using fitted cubic spline functions as the smooth background $I_0(k)$. It is crucial to use a consistent method of extracting χ [determining $I_0(k)$] for both experimental data and theoretical calculations to achieve satisfactory agreement between the two. The agreement between theory and experiment seen in Fig. 9 provides a strong

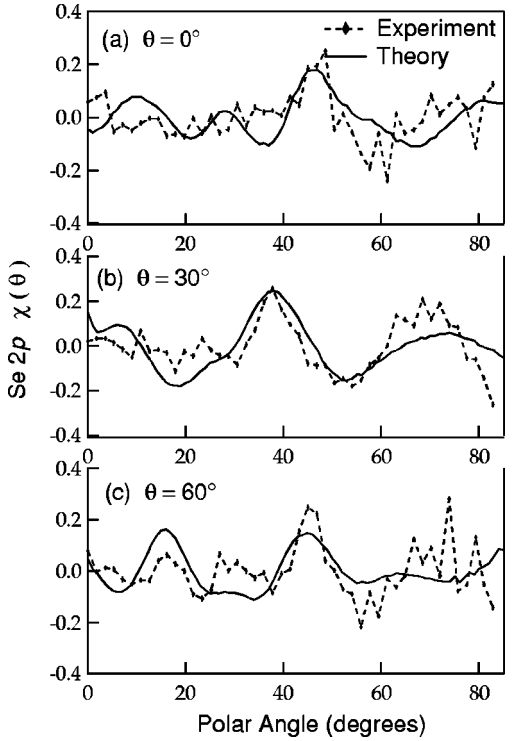

FIG. 10. Photoemission intensity modulations of Se $2p$ (KE $=48$ eV) core level on Si(111):GaSe along three high symmetry azimuths. 0°, 30°, and 60° correspond to $[11\bar{2}]$, $[10\bar{1}]$, and $[2\bar{1}\bar{1}]$ azimuths, respectively.

confirmation of the structure model in Fig. 5. In particular, the angular positions of the diffraction features are well reproduced, while the intensities less so. This likely reflects an averaging over static and dynamic disorder in the experiment, which affects multiple scattering paths involving several atoms more than those with only one or two scattering events.

Figure 10 shows experimental and theoretical results for low-energy (48 eV) Se $2p$ 3/2 emission as a function of polar angle for the same three azimuths, using Al K_α x rays ($h\nu=1486.6$ eV, binding energy ~ 1438 eV). The increased noise in the data compared to the corresponding Ga $2p$ pattern is due primarily to the rapidly rising background of inelastically scattered electrons at these low energies. For emission angles larger than about 45°, the inelastic background contributes more counts than does the Se $2p$ peak. The calculated diffraction curves satisfactorily reproduce the main data features using one fitting parameter, the inner potential, which is the difference between electron kinetic energies inside and outside the crystal. Generally, small changes in the inner potential do not make significant differences in calculated photoelectron diffraction patterns. However, this is no longer the case for the Se $2p$ data, where the inner potential is a significant fraction of the electron kinetic energy. Using this strong sensitivity of the Se $2p$ diffraction modulations, we determined the inner potential to be 13 ± 1 eV. This value is larger than that found with higher energy electrons (see Fig. 3), which may reflect a different effective muffin tin zero for these lower energy electrons that are more sensitive to the nonspherical part of the crystal potential. The lower k values probe larger distances from the atomic centers, since the relevant parameter is the product kr.

IV. SUMMARY

GaSe bilayer passivated Si(111) demonstrates a new mechanism of Si surface passivation by a III-VI compound. Ga forms the lower half of the bilayer bonding to Si, whereas Se forms the upper half of the bilayer, exposing a lone-pair state on the surface. The resulting fully saturated surface resembles Si(111):As.

We have applied low-energy photoelectron diffraction in various modes (scanned-energy PED, scanned-angle PED and stereogram) and with various x-ray sources (synchrotron and conventional laboratory x-ray source) to the GaSe bilayer passivated Si(111) system to probe the atomic bonding configuration between Ga and Si. We determined Ga sits directly atop of Si, as opposed to H_3 and T_4 configurations. The bilayer has a single domain and the Ga-Si bond length has been determined to be 2.35 Å, consistent with DFT calculations. Surface sensitive Si $2p$ core-level spectra show near-surface silicon atoms to be in a bulklike environment, with surface shift no more than 200 meV.

The different types of PED measurement provide us a variety of views toward the system under consideration and each holds its own merit. In particular, scanned-energy PED is effective in probing the bond length and bonding geometry between overlayer and substrate, whereas the diffraction stereogram gives a more complete view of the structural environment surrounding the emitting atom. Low-energy scanned-angle PED of deep core-level emission can be effectively carried out using conventional laboratory x-ray source setup. The results, although often more subtle and intricate, provide equivalent information about the interface structure between the overlayer and substrate. In all of the above processes, sophisticated multiple-scattering modeling is critical in drawing reliable conclusions from the experimental measurement. We also find that the modeling software (FEFF and MSCD) developed and tested primarily for metallic systems works well for this covalently bonded surface.

ACKNOWLEDGMENTS

We gratefully acknowledge J. J. Rehr and A. L. Ankudinov at the University of Washington for discussions concerning theoretical modeling and providing the *ab initio* FEFF code, Y. Chen and M. A. Van Hove at Lawrence Berkeley National Laboratory for providing the photoelectron diffraction modeling package MSCD, and Kurt Schroeder at Forschungszentrum Jülich for performing the DFT calculation. This work was supported by NSF Grant No. DMR9801302. Experiments were performed at the Advanced Light Source of Lawrence Berkeley National Laboratory operated by the U.S. DOE under Contract No. DE-AC03-76SF00098.

[1] K. Takayanagi, Y. Tanishiro, S. Takahashi, and M. Takahashi, Surf. Sci. **164**, 367 (1985).
[2] H. Ibach and J.E. Rowe, Surf. Sci. **43**, 481 (1974).
[3] G.S. Higashi, Y.J. Chabal, G.W. Trucks, and K. Raghavachari, Appl. Phys. Lett. **56**, 656 (1990).
[4] K. Itaya, R. Sugawara, Y. Morita, and H. Tokumoto, Appl. Phys. Lett. **60**, 2534 (1992).
[5] M.A. Olmstead, R.D. Bringans, R.I.G. Uhrberg, and R.Z. Bachrach, Phys. Rev. B **34**, 6041 (1986).
[6] R.I.G. Uhrberg, R.D. Bringans, M.A. Olmstead, R.Z. Bachrach, and J.E. Northrup, Phys. Rev. B **35**, 3945 (1987).
[7] S. Meng, B.R. Schroeder, and M.A. Olmstead, Phys. Rev. B **61**, 7215 (2000).
[8] Y. Zheng, A. Koëbel, J.F. Pétroff, J.C. Boulliard, B. Capelle, and M. Eddrief, J. Cryst. Growth **162**, 135 (1996).
[9] A. Koëbel, Y. Zheng, J.F. Pétroff, J.C. Boulliard, B. Capelle, and M. Eddrief, Phys. Rev. B **56**, 12 296 (1997).
[10] M. A. Olmstead, A. Bostwick, S. Meng, J. A. Adams, E. Rotenberg, F. S. Ohuchi, R. Rudolf, C. Pettenkofer, R. Fritsche, A. Klein, and W. Jaegermann (unpublished).
[11] J. A. Adams, A. Bostwick, S. Meng, B. R. Schroeder, M. A. Olmstead, and F. S. Ohuchi (unpublished).
[12] R. Rudolph, C. Pettenkoffer, A. Klein, and W. Jaegermann, Appl. Surf. Sci. **167**, 122 (2000).
[13] F. S. Ohuchi and M. A. Olmstead, in *Wiley Encyclopedia of Electrical and Electronics Engineering*, edited by J. G. Webster (Wiley, New York, 1999), Vol. 19, p. 147.
[14] K.Y. Liu, K. Ueno, Y. Fujikawa, K. Saiki, and A. Koma, Jpn. J. Appl. Phys. **32**, L434 (1993).
[15] L.T. Vinh, M. Eddrief, C. Sébenne, A. Sacuto, and M. Balkanski, J. Cryst. Growth **135**, 1 (1994).
[16] J.E. Palmer, T. Saitoh, T. Yodo, and M. Tamura, J. Cryst. Growth **147**, 283 (1995).
[17] A. Koëbel, Y. Zheng, J.F. Pétroff, M. Eddrief, L.T. Vinh, and C. Sébenne, J. Cryst. Growth **154**, 269 (1995).
[18] N. Jedrecy, R. Pinchaux, and M. Eddrief, Phys. Rev. B **56**, 9583 (1997).
[19] R. Rudolph, C. Pettenkoffer, A. Klein, and W. Jaegermann, Appl. Surf. Sci. **166**, 437 (2000).
[20] K. Schroeder (FZ-Jülich) (private communication).
[21] Y. Chen, F.J. García de Abajo, A. Chassé, R.X. Ynzunza, A.P. Kaduwela, M.A. Van Hove, and C.S. Fadley, Phys. Rev. B **58**, 13 121 (1998).
[22] J.J. Rehr and R.C. Albers, Phys. Rev. B **41**, 8139 (1990).
[23] J. Mustre de Leon, J.J. Rehr, S.I. Zabinsky, and R.C. Albers, Phys. Rev. B **44**, 4146 (1991).
[24] J.J. Rehr and R.C. Albers, Rev. Mod. Phys. **72**, 621 (2000).
[25] R.D. Bringans, M.A. Olmstead, R.I.G. Uhrberg, and R.Z. Bachrach, Appl. Phys. Lett. **51**, 523 (1987).
[26] T. Hanada, H. Daimon, S. Nagano, S. Ino, S. Suga, and Y. Murata, Phys. Rev. B **55**, 16 420 (1997).
[27] R.L. Headrick and W.L. Graham, Phys. Rev. B **37**, 1051 (1988).
[28] M. Copel and R.M. Tromp, Phys. Rev. B **37**, 2766 (1988).
[29] R.E. Martinez, E. Fontes, J.A. Golovchenko, and J.R. Patel, Phys. Rev. Lett. **69**, 1061 (1992).